Development. 2013 Jan 15;140(2):313–322. doi: 10.1242/dev.086900

Bioelectric signaling regulates head and organ size during planarian regeneration

Wendy Scott Beane [1], Junji Morokuma [1], Joan M Lemire [1], Michael Levin [1,*]

Author information Article notes Copyright and License information

PMCID: PMC3597208 PMID: 23250205

Abstract

A main goal of regenerative medicine is to replace lost or damaged tissues and organs with functional parts of the correct size and shape. But the proliferation of new cells is not sufficient; we will also need to understand how the scale and ultimate form of newly produced tissues are determined. Using the planarian model system, we report that membrane voltage-dependent bioelectric signaling determines both head size and organ scaling during regeneration. RNA interference of the H^+,K^+-ATPase ion pump results in membrane hyperpolarization, which has no effect on the amount of new tissue (blastema) that is regenerated yet produces regenerates with tiny ‘shrunken’ heads and proportionally oversized pharynges. Our data show that this disproportionality results from a lack of the apoptosis required to adjust head and organ size and placement, highlighting apoptotic remodeling as the link between bioelectric signaling and the establishment of organ size during regeneration.

Keywords: H,K-ATPase; Apoptosis; Bioelectricity; Morphogenesis; Planaria; Regeneration; Size control; *Schmidtea mediterranea*

INTRODUCTION

Numerous medically significant processes require the precise control of complex shape changes and tissue remodeling. Embryonic gastrulation movements transform a single cell layer into multiple germ layers (Nowotschin and Hadjantonakis, 2010), whereas during metamorphosis entire body plans are abandoned in favor of completely different ones (Pastor-Pareja et al., 2004). Extracellular matrix remodeling accompanies metastatic progression in cancer (Egeblad et al., 2010), and airway remodeling results from both injury (e.g. cigarette smoke) and disease (e.g. asthma) (Huang et al., 2008; Rydell-Tormanen et al., 2012). Remodeling even plays a central role during aging in tissues such as bone (Gosman et al., 2011). But despite the importance of tissue remodeling, we do not yet understand the mechanisms that coordinate individual cell regulatory pathways into tissue- and organ-level organization. Understanding and learning to control the processes determining proportion during organism-wide tissue scaling is a paradigm case of a fundamental problem in systems biology.

For regenerative medicine, which aims to replace lost or damaged organs and limbs, elucidating these mechanisms is crucial because the production of new cells is not sufficient – new tissues must be the correct size and shape to restore form and function. Likewise, addressing malformations from birth defects requires the functional manipulation of multicellular structures, not merely the induction of differentiation or proliferation of distinct cell types. Planaria are a powerful model for such studies: they can regenerate any body structure after damage, and two centuries of observation has precisely detailed the morphological changes they undergo during regeneration (Newmark and Alvarado, 2001). Recent work has begun to elucidate the molecular mechanisms underlying maintenance of their adult stem cell population (Wagner et al., 2011; Wagner et al., 2012), wound-induced injury responses (Petersen and Reddien, 2009; Wenemoser et al., 2012), proliferation of new tissues (Wenemoser and Reddien, 2010), polarity assignment of the new tissue (the blastema) (Reddien, 2011) and stem cell differentiation in regenerating tissues (Eisenhoffer et al., 2008).

Crucially, original tissues are dynamically remodeled concurrently with new tissue growth during planarian regeneration. Thus, relative tissue proportions are maintained to current body size through allometric scaling of pre-existing structures (Oviedo et al., 2003). Thomas Hunt Morgan termed regenerative tissue remodeling or the rearrangement of existing cells ‘morphallaxis’, delineating it from epimorphic regeneration mainly dependent on new proliferation (Morgan, 1901). However, the signals that direct the scale and geometry of morphallactic remodeling relative to new tissue growth during regeneration remain unidentified. Understanding the highly regulative, flexible patterning programs of vertebrate development and the reparative pathways of regeneration requires that the molecular mechanisms underlying size and shape controls be analyzed in tractable model systems such as planaria. Although planarian research has focused on blastema formation, stem cell regulation, and polarity (head

versus tail decisions), we still lack genetic entry points into how remodeling events are coordinated with predetermined 'templates' that give rise to the same shape time and time again.

Regenerative repair of complex structures is often accomplished in part by programmed cell death or apoptosis (Fuchs and Steller, 2011); for example, apoptosis is required for proliferative outgrowth during *Xenopus* tail regeneration (Tseng et al., 2007) and head regeneration in *Hydra* is initiated by apoptosis-mediated Wnt signaling (Chera et al., 2009). We report here that the H^+,K^+-ATPase (H,K-ATPase) ion transporter regulates tissue remodeling via apoptosis during planarian regeneration. Our previous work revealed a role for H,K-ATPase in specifying anterior polarity in new tissues (Beane et al., 2011). In the present work, we demonstrate that H,K-ATPase is also required for head size and organ proportionality during regeneration, by mediating the apoptotic sculpting of original tissues. These molecular data for the first time link a bioelectric pathway determining anatomical polarity with cellular mechanisms that regulate shape determination and allometric scaling during regeneration.

MATERIALS AND METHODS

Cloning

Homologs to H^+,K^+-ATPase (H,K-ATPase) were used to search (tBlastn) the *Schmidtea mediterranea* Genome Database (Robb et al., 2008). To confirm H,K-ATPase identity, the seven planarian sequences co-identified by multiple homologs were used to search (tBlastx) NCBI BLAST (http://blast.ncbi.nlm.nih.gov/Blast.cgi) and protein domain analyses were performed using both the NCBI Conserved Domains Database (http://www.ncbi.nlm.nih.gov/cdd) and SMART (http://smart.embl-heidelberg.de). An *S. mediterranea* cDNA library (from intact worms) was used to generate initial gene fragments by PCR with primers designed by Primer3 (http://frodo.wi.mit.edu/primer3). Because in invertebrates it is not possible to delineate between the two closely related P2C class plasma membrane ATPases Na^+,K^+-ATPase and H,K-ATPase, all potential candidates for either gene were identified. Primers used were (other candidates identified by their *S. mediterranea* Genome Database locus id): *Smed-H¸K-ATPase*: 5′-GCAATGAAAGGTGCCCCAGAAAGAA, 3′-GC AAGAGAAATAGCGGGCACCATGT; Candidate v31.000529: 5′-TGTCACGGCCACCAAGGAATATCAA, 3′-CGTAGCACGTTTTCACACGGAGCAT; Candidate v31.001001: 5′-ACATCGCTGTGTCGATCCCCTTACC, 3′-TAAAATGAGGTCCATCCCGGGACAA; Candidate v31.021250: 5′-TCGCTAATCTCGCAAGTGGTCTGGA, 3′-AAGCGCCTCGTCTTCTTCTGATTGA; Candidate v31.002299: 5′-TGGGATTGTCTGGTTCCGATGTCAG, 3′-CATTAATGGCCGGTGAATCCCACTC; Candidate v31.000996: 5′-GATCGGATCCCGGCAGATGTTAGAA, 3′-AGCATTCCTTCCGGAACATTGGCTA.

Using the PCR fragments obtained, RNAi regeneration phenotypes and intracellular pH analyses were used to distinguish potential H,K-ATPase(s) from potential Na,K-ATPases, after which a single non-gastric H,K-ATPase alpha subunit was identified. Regeneration phenotypes for other candidates: v31.000529, none; v31.001001, inchworm-like movements; v31.021250, death; v31.002299, death; v31.000996, eye variations. For *Smed-H¸K-ATPase*, the full-length gene sequence was then obtained using Smart/er RACE cDNA Amplification Kits (Clontech), from 5′ and 3′ RACE cDNAs generated as described in the kit. *Smed-H¸K-ATPase* GenBank accession number: JX174182. Alignments were generated using MultAlin (Corpet, 1988). Protein domain alignments were generated using the NCBI Conserved Domains Database.

Colony care and amputations

The CIW4 clonal line of asexual *S. mediterranea* was used and maintained at 20°C in the dark in 1× Montjuïc salts as previously described (Cebria and Newmark, 2005). Worms 4-7 mm long were starved for ≥1 week prior to use. Amputations were performed under a dissecting microscope with a scalpel, on filter paper over a moist Kimwipe kept chilled on a cold plate. Pharynx fragments were produced by cutting just above and just below the pharynx. Fragments were kept in welled non-treated tissue-culture plates in the dark at 19°C, and moved into fresh media and new wells once a week, until scored. For all membrane voltage and intracellular pH assays, pharynx regenerates were produced as above, except either the anterior or posterior cut was slanted at a 45° angle (equal numbers of each cut were made; only anterior slants shown). This provided an internal reference for the original anterior-posterior axis, to positively establish the identity of each blastema.

RNA interference (RNAi) and pharmacology

For RNAi experiments, dsRNA was generated and injected as described by Oviedo et al. (Oviedo et al., 2008). Control dsRNA was Venus-GFP. Worms were injected on days 1-3 and cut on day 8 or 14. The apoptosis inducer staurosporine (Calbiochem) was used at 20 nM. The apoptosis inhibitor M50054 (Calbiochem 178488) was used at 80 µM. All stocks were suspended in DMSO; DMSO controls (shown) had no effect.

In situ hybridization and immunofluorescence

Worms for whole-mount *in situ* hybridization were formalin fixed (or Carnoy's fixed for *Inx9*), and *in situ* hybridizations were performed as described by Pearson et al. (Pearson et al., 2009). Probes: *Cintillo* (Oviedo et al., 2003); *Inx9* (Oviedo and Levin, 2007); *sFRP-1* and *Wnt11-5*, kind gifts of P. Reddien (Petersen and Reddien, 2008). Worms for immunofluorescence were Carnoy's fixed and antibody stained

as described (Beane et al., 2012). Primary antibodies were: α-phosphorylated histone H3 (H3P), 1:250 (Upstate); α-synapsin, 1:50 (Developmental Studies Hybridoma Bank); acetylated tubulin, 1:1000 (Sigma T7451); activated caspase-3, 1:1000 (Abcam ab13847); and α-arrestin, 1:10,000 (kind gift from K. Watanabe, University of Hyogo, Japan). Secondary antibodies were: goat anti-mouse Alexa488, 1:400 (Sigma) or (for H3P and caspase-3) an HRP-conjugated anti-rabbit antibody with TSA-Alexa568 anti-HRP (Molecular Probes).

Membrane voltage, pH_i reporter, and behavioral assays

$DiBAC_4(3)$ (bis-[1,3-dibarbituric acid]-trimethine oxanol) (Invitrogen), suspended in DMSO, was used at 0.475 μM to measure voltage; the ratiometric dye SNARF-5F-AM (Molecular Probes S-23923), suspended in DMSO with 20% w/v Pluronic F-127, was used at 5 μM to measure intracellular pH; both as previously described (Beane et al., 2011) using 3% EtOH-immobilized worms (Stevenson and Beane, 2010). Movements were quantified with a custom-made computer vision system (Hicks et al., 2006; Blackiston et al., 2010). Ten minute trials in the dark were recorded at 5 Hz. Occupancy heat maps and area covered data were generated with J-Specimen (Ebiotics).

Image collection, measurements and statistics

Images were collected using either a Nikon SMZ1500 microscope with a Retiga 2000R camera (Q-Imaging) and Q-Capture imaging software; or an Olympus BX61 compound microscope with a Hamamatsu Orca AG CCD camera and IP Labs or MetaMorph imaging software. Quantify segment tool (IP Labs) was used to measure fluorescence pixel intensity. Adobe Photoshop was used to orient and scale images, and improve clarity (not for V_{mem} or pH_i images). Data were neither added nor subtracted; original images available upon request. Microsoft Excel was used to calculate Student's *t*-test (two-tailed distribution, two independent samples, unequal variance). Error bars are standard deviation.

All measurements were carried out using images of worms when fully extended to prevent introducing 'noise' into our calculations from worms that appeared to have wider body shapes owing to 'scrunching' or thinner body shapes (especially in the head) from partial stretching of the body. Photoshop was used for measurements (in pixels) of area (magnetic lasso tool) and distance, length and width (ruler tool). Head size was calculated as (area of head)/(area of worm), with the auricles (for morphological analyses) or the posterior-most cintillo expression (for molecular analyses) providing the posterior boundary. Blastema size was calculated only by morphology as (area of blastema)/(area of worm), using the region of unpigmented tissue on 4 days post-amputation (dpa) as blastema area. Pharynx size was calculated as (area of pharynx)/(area of worm), with the ring of darkened pigment (for morphological analyses) and the borders of the synapsin-labeled pharyngeal neural plexus (for molecular analyses)

determining area boundaries. Pharynx location was calculated as (length from the anterior tip of the pharynx to the anterior tip of the worm)/(square root of area of worm) for both morphological and molecular analyses. For all these calculations, measurements were controlled (by including total worm area) for differences in individual body sizes between worms, which can vary greatly. For measurements of body elongation, morphological analyses of worm width (on the medial-lateral axis) was calculated at the widest point on fully extended worms (with all images at the same magnification). For 0 dpa and 3 dpa fragments (which do not typically extend), width was measured at the midpoint of the pharynx. For calculations over time, the same individual worms were followed over the course of each assay, and the differences for each single worm were calculated prior to averaging numbers for the entire experiment.

RESULTS

Planarians undergo regulated tissue remodeling during regeneration

For the purposes of this study, we defined epimorphic regeneration as the cell proliferation and migration associated with formation of the unpigmented blastema (or new tissue), whereas morphallactic regeneration was defined as the cell rearrangements that restore proportionality in the pre-existing pigmented fragment (or old tissue) largely without new proliferation. Molecular analyses of organism-wide morphallaxis are lacking for planarians, although a recent study has analyzed remodeling of the intestines (Forsthoefel et al., 2011). Therefore, establishing a baseline for detecting morphallactic changes was crucial. Pre-existing tissue remodeling during planarian regeneration is completed within ~3 weeks after amputation (Gonzalez-Estevez et al., 2007; Forsthoefel et al., 2011). Although all tissues and organs are remodeled during this process, the most dynamic morphological reorganizations involve maintaining head and pharynx proportions and pharyngeal location. We used *cintillo*, expressed in a ring of putative chemoreceptor neurons surrounding the head (Oviedo et al., 2003), to demarcate the head region, and anti-synapsin labeling of the pharyngeal neural plexus was used to delineate the pharynx (Fig. 1A). This enabled us to assess changes in remodeling by both morphological and molecular analyses (Fig. 1B), with percentages reported as an average of both methods.

Fig. 1.

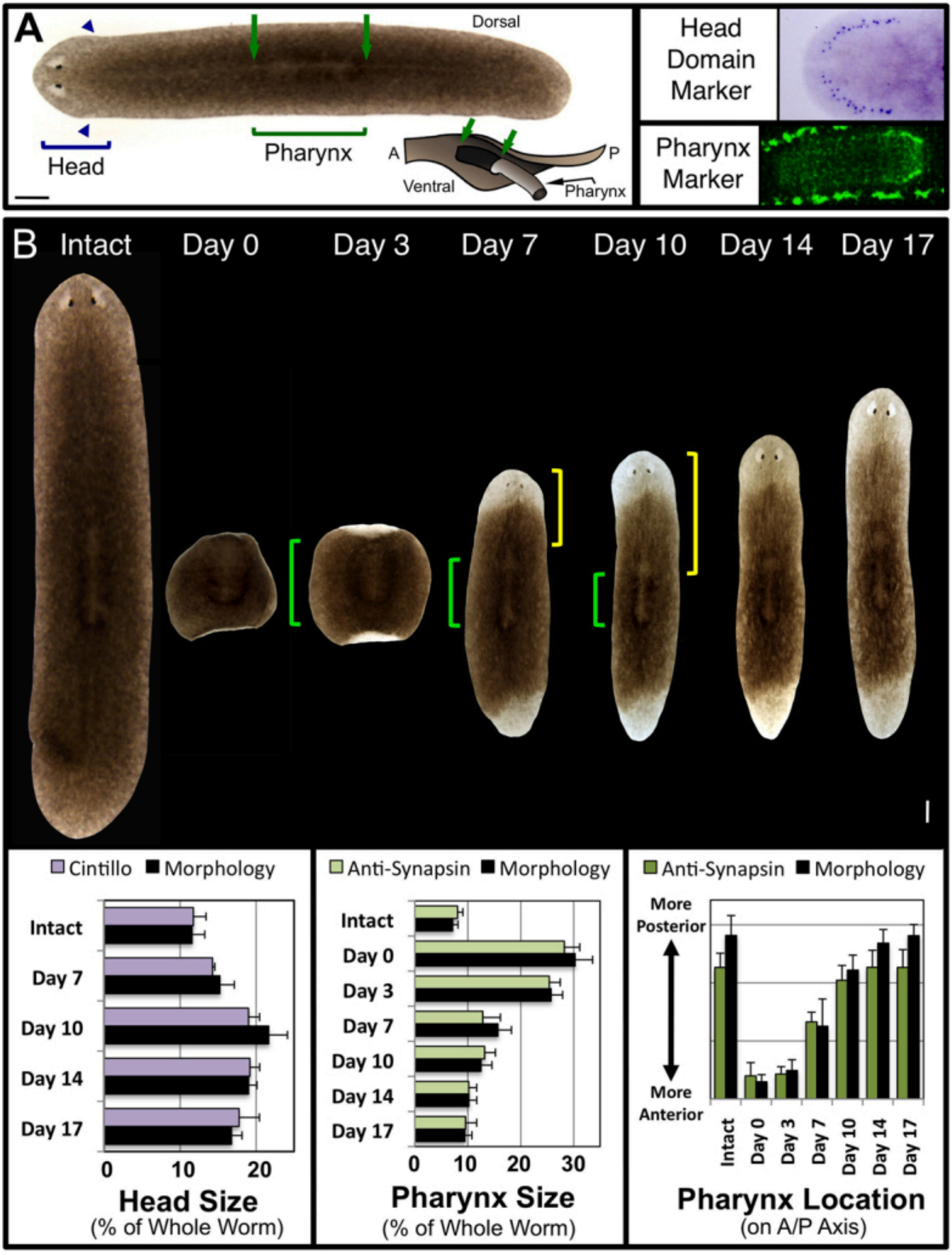

Open in a new tab

Characterization of tissue remodeling during planarian regeneration. (**A**) Intact *S. mediterranea*. Brackets: regions used for morphological analyses. Posterior boundary of the head marked by the auricles (arrowheads). Pharynx dorsally viewed as a lightly pigmented region outlined by a ring of darker pigment (arrows). Inset: diagram of pharynx extended through ventral pharyngeal opening (A, anterior; P, posterior). Molecular markers: head domain, *Smed-cintillo*; pharynx, anti-synapsin (pharyngeal nerve plexus bordered top and bottom by the ventral nerve cords). Anterior is left. (**B**) Composite image of regeneration over 17 days in a single planarian pharynx regenerate (amputated just anterior and posterior to the pharynx). Green brackets, pharynx; yellow brackets, distance between pharynx and tip of the head (pharynx location on the A/P axis). Anterior is up. Quantification of tissue remodeling by both morphological and molecular analyses (in the same regenerates over time for morphology) are shown below. Error bars: s.d. ($n \geq 10$). Scale bar: 200 µm.

We examined head and pharynx size as a percentage of the whole worm to control for differences in worm size (which varies between individuals). Pharynx location was measured as the distance from the top of the worm to the anterior tip of the pharynx (Fig. 1B, yellow brackets), divided by the square root of total worm area (again to control for worm size). In whole worms, the head region was on average 11.7% of the entire worm, whereas the pharynx averaged 7.6% and was located in (or just posterior to) the center of the anterior-posterior (A/P) axis (Fig. 1B). With these baselines established, we analyzed remodeling in pharynx regenerates by amputating worms just anterior, and just posterior, to the pharynx (Fig. 1B). These cuts produced fragments that retained their original pharynx, which now extended almost the entire length of the fragment. This allowed us to follow remodeling of the original pharynx as it shrinks and moves posteriorly on the A/P axis, as well as the process of head regeneration in tissues that originally had a more posterior polarity.

We tracked individual worms from their intact (uncut) state through 17 days post-amputation (dpa). Little to no remodeling was observed before 3 dpa, consistent with the regenerate's early focus on injury response and blastema formation. Rescaling pharynx size (Fig. 1B, green brackets) to the worm's new, smaller size was largely (75.9%) finished by 7 dpa. By 17 dpa, the pharynx was reduced by 19.7% from its original size (supplementary material Fig. S1A). Pharynx relocation towards the posterior was mostly (81.4%) completed by 10 dpa. The head region (as a percentage of the whole worm), instead of just growing from the blastema to the correct proportion, increased by 10 dpa to 74.4% larger than in intact animals. Only after 10 dpa did the head begin to scale down towards its smaller, baseline percentage, although our data indicate that this process was only 57.1% completed by 17 dpa. These data suggest that pharynx remodeling is largely completed by 10 dpa, whereas scaling of the new head (following new tissue growth) does not occur until after the pharynx remodeling is finished.

The final morphallactic event we analyzed was the rapid and reliable transformation of pharynx fragments from a wide, square shape to the thin, elongated typical planarian form (Fig. 1B). Over 17 days, regenerates reduced their width along the mediolateral axis by a total of 48.8% as elongation of the entire worm occurred. The majority (51.8%) of this elongation was accomplished by 7 dpa, concurrent with pharynx resizing. From 10 to 14 dpa, little body lengthening was observed; most of the remaining elongation occurred after 14 dpa, concurrent with the reduction in head size. Having quantified this remarkable combination of morphallactic events in control animals, we next sought to probe the molecular mechanisms involved.

H,K-ATPase inhibition blocks membrane depolarization and pharyngeal scaling

In our work with the *Dugesia japonica* planaria, we observed that chemical inhibition of the H,K-ATPase ion transporter (through regulation of blastema membrane voltage) blocked anterior polarity and head regeneration without preventing blastema growth (Beane et al., 2011). However, we also observed that regenerates had abnormally wide bodies, with very large pharynges that were atypically anterior. This suggested a lack of remodeling in these regenerates. To identify the genetic mechanisms behind this regenerative shape failure, we identified from the more genetically tractable *Schmidtea mediterranea* species a single homolog of the alpha subunit of the non-gastric H,K-ATPase, which had the same domain architecture and 69.9% pairwise identity to vertebrate homologs (supplementary material Fig. S2). Interestingly, RNA interference (RNAi) of the *Smed-H¸K-ATPase* produced pharynx regenerates that not only displayed the large, anteriorly shifted pharynges noted previously, but, surprisingly, also had tiny, shrunken heads (Fig. 2A). Although *Smed-H¸K-ATPase(RNAi)* injection did produce a consistently small number of headless regenerates (4.2%), similar to H,K-ATPase inhibition in *D. japonica* (supplementary material Fig. S3), the majority of regenerates (91.6%) regenerated with proportionally very tiny heads. This ‘shrunken head’ phenotype has not to our knowledge been reported from any other perturbation to date, and is consistent with tissue remodeling defects following loss of H,K-ATPase activity.

Fig. 2.

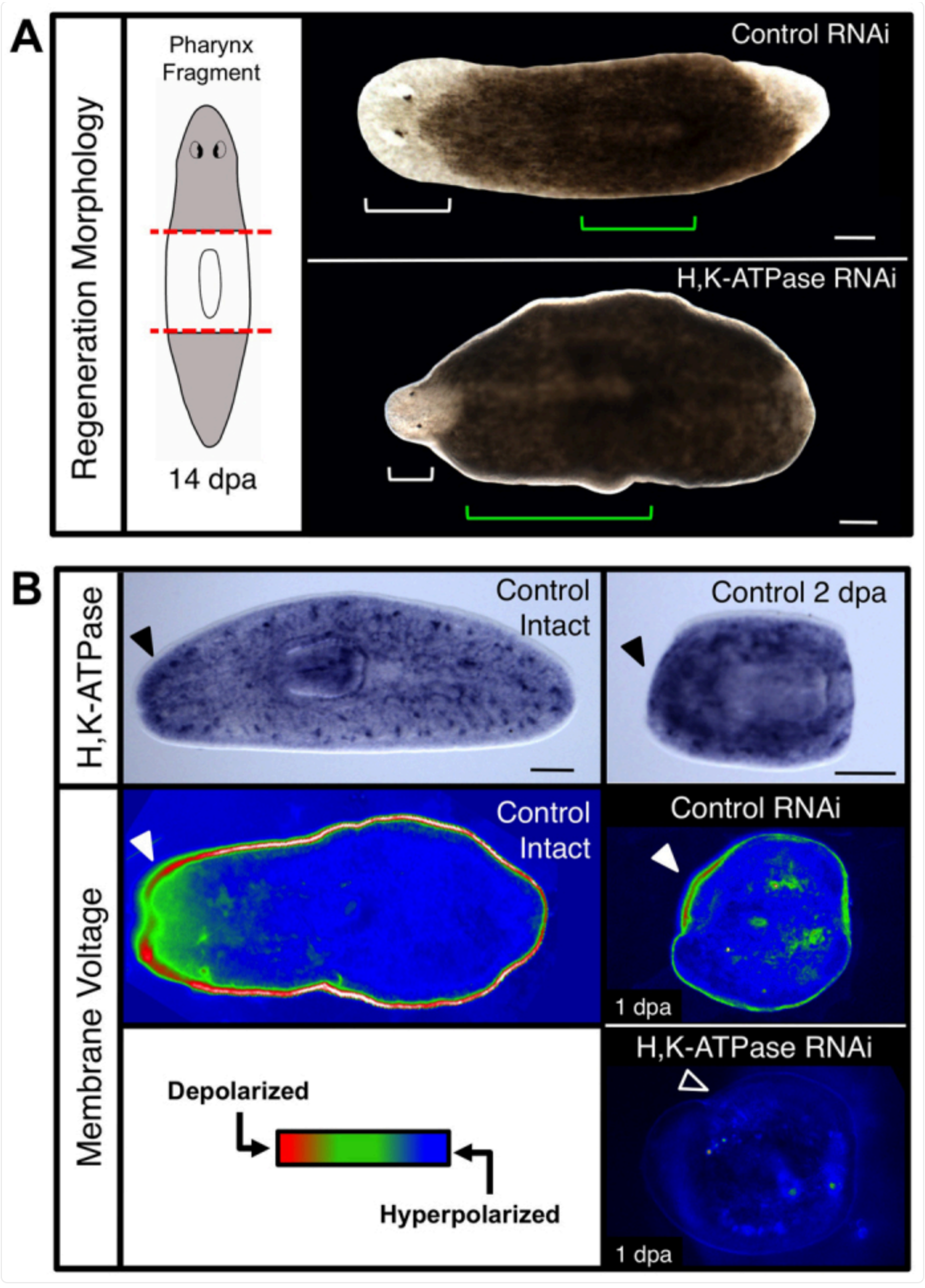
A
Regeneration Morphology
Pharynx Fragment
14 dpa
Control RNAi
H,K-ATPase RNAi
B
H,K-ATPase
Control Intact
Control 2 dpa
Membrane Voltage
Control Intact
Control RNAi
1 dpa
Depolarized
Hyperpolarized
H,K-ATPase RNAi
1 dpa

Open in a new tab

The H,K-ATPase ion pump regulates membrane voltage and regenerative scaling. (**A**) Pharynx fragments at 14 dpa following H,K-ATPase inhibition by RNAi. Red dashed lines, amputation planes; white brackets, head; green brackets, pharynx. Shrunken head phenotype: 91.6%. $n \geq 125$. (**B**) H,K-ATPase expression leads to membrane depolarization in intact worms and pharynx regenerates. Top: *In situ* hybridization showing *Smed-H*$_{\beta}$*K-ATPase* expression, $n > 5$. Black arrowheads denote upregulated anterior expression. Middle and bottom: Membrane voltage reporter assay using $DiBAC_4(3)$, $n > 10$. Red, relatively depolarized; blue, relatively hyperpolarized. Filled arrowheads denote presence and unfilled arrowhead absence of anterior depolarization. Anterior is left. Scale bars: 200 μm.

To confirm the transporter identity of *Smed-H*$_{\beta}$*K-ATPase*, the intracellular pH of RNAi-injected animals was assayed, confirming that inhibited worms were acidified from cytoplasmic proton retention (supplementary material Fig. S4A). *In situ* hybridization (Fig. 2B) revealed H,K-ATPase expression throughout untreated worms, with punctate areas of high expression particularly at the lateral margins. During regeneration, H,K-ATPase expression occurred first in the anterior, then in both, blastemas, but always greater in the anterior (Fig. 2B; supplementary material Fig. S4B). In intact animals, the anterior region is highly depolarized compared with the rest of the animal, corresponding to an upregulated region of H,K-ATPase expression delineating the head region (Fig. 2B). In regenerates, by 24 hours post-amputation (hpa) the anterior blastema becomes strongly depolarized (Fig. 2B). Following H,K-ATPase RNAi, this depolarization is lost; the entire regenerate was strongly hyperpolarized by 24 hpa (Fig. 2B) and remained hyperpolarized throughout regeneration (supplementary material Fig. S4C). Thus, *Smed-H*$_{\beta}$*K-ATPase* is in the ideal spatiotemporal position to regulate the membrane voltage of the anterior blastema during regeneration, as well as the process of morphallaxis throughout the animal.

Pre-existing tissues retain their original identity without H,K-ATPase

We next performed marker analyses of *Smed-H*$_{\beta}$*K-ATPase(RNAi)* shrunken-headed pharynx regenerates. Nervous system labeling (Fig. 3A) highlighted the atypical anterior pharynx position of H,K-ATPase-inhibited regenerates, and revealed that both new brain (in the anterior) and ventral nerve cord (in the posterior) growth had occurred. However, the brains of shrunken-headed regenerates lacked most of their neural tissue (Fig. 3A, insets). Analysis of the visual neurons showed that although photoreceptor cells did regenerate, their innervation was highly defective (supplementary material Fig. S5). This neuronal deficiency was supported by quantitative behavior analyses demonstrating a lack of exploratory

behavior in both intact and regenerate H,K-ATPase-inhibited worms (supplementary material Fig. S6A), which failed to move despite having the cilia used for locomotion (supplementary material Fig. S6B). This is consistent with previous reports that neural defects (such as in dopaminergic neurons) affect movement in planarians (Nishimura et al., 2007), locomotion of which has been shown to be both cilia and muscle dependent. Together, these data suggest that in *Smed-H¸K-ATPase(RNAi)* animals incomplete brain regeneration disrupts function.

Fig. 3.

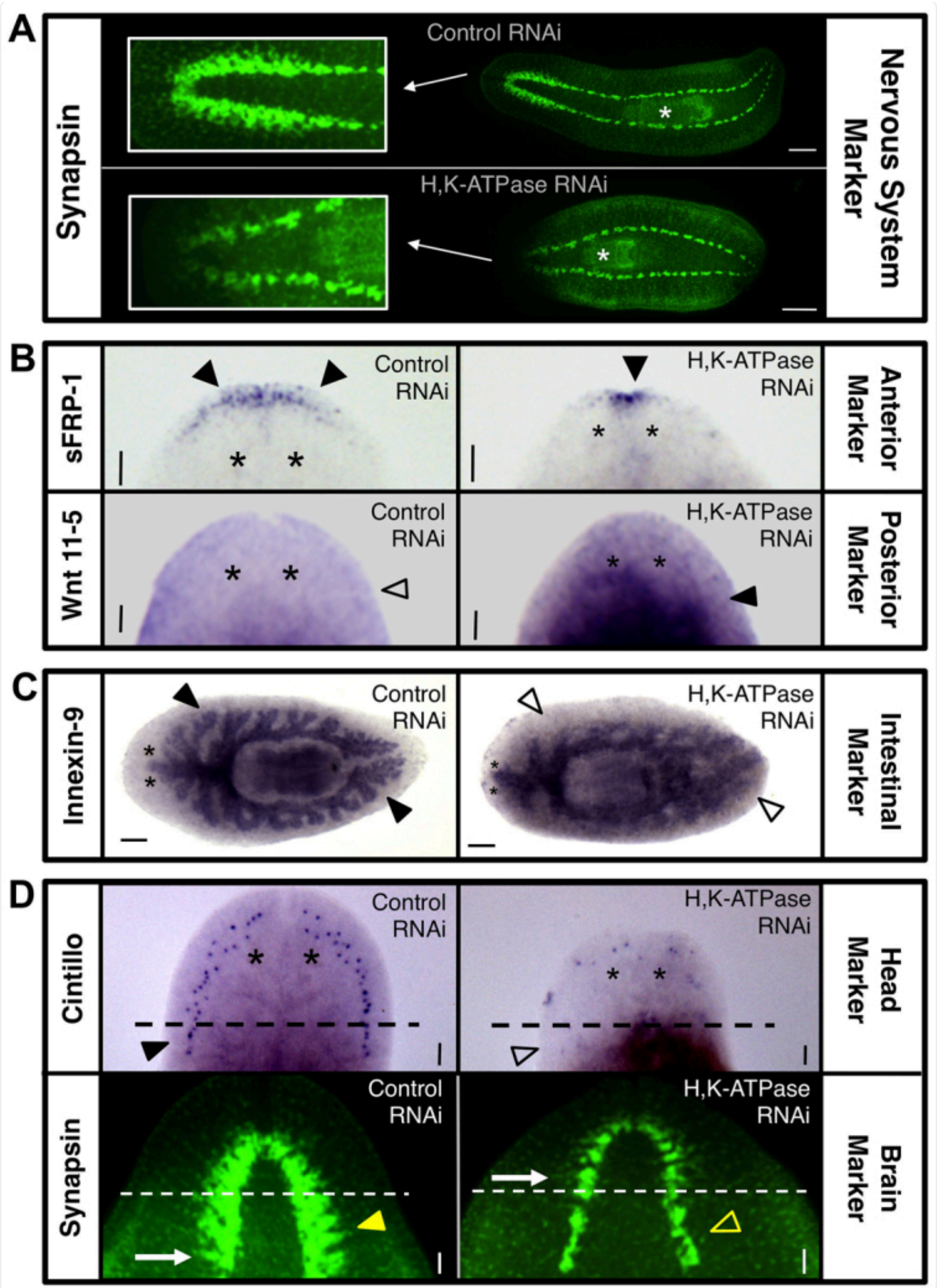
A
Synapsin
Control RNAi
H,K-ATPase RNAi
Nervous System Marker
B
sFRP-1
Control RNAi
H,K-ATPase RNAi
Anterior Marker
Wnt 11-5
Control RNAi
H,K-ATPase RNAi
Posterior Marker
C
Innexin-9
Control RNAi
H,K-ATPase RNAi
Intestinal Marker
D
Cintillo
Control RNAi
H,K-ATPase RNAi
Head Marker
Synapsin
Control RNAi
H,K-ATPase RNAi
Brain Marker

Open in a new tab

H,K-ATPase is required for remodeling tissue identities during regeneration. Marker analyses in 14 dpa pharynx regenerates (unless otherwise noted). (**A**) Nervous system analysis by anti-synapsin labeling ($n=10$). Insets: closeup of brain. White asterisks indicate pharynx. (**B**) Anterior-posterior polarity analyses of head region ($n\geq7$). Anterior marker: *sFRP-1*. Posterior marker: *Wnt 11-5*. Filled arrowheads denote presence and unfilled arrowhead absence of expression. (**C**) Intestinal tract analysis by *Innexin-9* staining ($n\geq6$). Filled arrowheads denote presence and unfilled arrowheads absence of tertiary intestinal branching. (**D**) Analyses of new tissue versus pre-existing tissue gene expression ($n\geq9$). Head domain marker: *cintillo*. Average number of *cintillo* dots: 40.2 (control), 13.7 (H,K-ATPase RNAi), $P<0.0001$. Brain marker: synapsin (10 dpa). Dashed lines: amputation plane. Filled arrowhead denotes presence and unfilled arrowhead absence of expression in pre-existing tissues. Arrows indicate posterior-most brain branch. Anterior: left (A,C) or up (B,D). White asterisks: pharynx. Black asterisks indicate position of eyes. Scale bars: in A, 200 µm; in C, 100 µm; in B,D, 50 µm.

Anterior marker analysis revealed that H,K-ATPase-inhibited pharynx fragments with shrunken heads also had greatly reduced anterior gene expression (Fig. 3B). Posterior marker analysis showed a corresponding increase in the area of posterior identity following H,K-ATPase inhibition, with posterior expression extending atypically all the way to the border of the shrunken head (Fig. 3B). As these regenerates initially had posterior expression throughout the entire fragment, this suggests that pre-existing tissues have retained their original posterior identity. Previous data showed that in posterior fragments the marker *Wnt 11-5* recedes from the new anterior edge over time (beginning ~3 dpa) concurrent with tissues remodeling to an anterior identity (Petersen and Reddien, 2009). Our data suggest that only the *de novo* tissues of the shrunken head become anterior following H,K-ATPase inhibition, whereas the existing tissues fail to remodel their posterior identity in line with their new position on the A/P axis.

Meticulous analyses in planarians have shown that both new growth and remodeling of pre-existing tissues play a role in regenerative patterning of the intestines (Forsthoefel et al., 2011). Intestinal tract analysis in *Smed-H,K-ATPase(RNAi)* pharynx regenerates revealed that, similar to the nervous system, new growth occurred but intestinal patterning was incomplete (Fig. 3C). The planarian intestinal (gastrovascular) tract comprises a single anterior and two posterior primary branches; from these, secondary branches diverge, which then divide into smaller tertiary and quaternary branches (Forsthoefel et al., 2011). In H,K-ATPase-inhibited regenerates, the primary intestine branch extended anteriorly into the shrunken head; however, fewer secondary branches were observed. In the posterior,

no secondary branches were seen in the new tissue. Throughout the intestinal tract, H,K-ATPase-inhibited regenerates lacked evidence of tertiary branching, except in the pre-existing tissues flanking the pharynx. These data demonstrate that intestinal remodeling also requires H,K-ATPase. Together, the marker analyses revealed that without H,K-ATPase activity, regenerating tissues retain their original identity, providing a basis for the phenotypically wide bodies and large pharynges observed.

H,K-ATPase is required for tissue remodeling but not new growth

The data suggest H,K-ATPase inhibition permits new growth (blastema) but not remodeling of existing tissues. To test this hypothesis, we closely examined the head region in *Smed-H,K-ATPase(RNAi)* regenerates (Fig. 3D). Analyses of the head domain marker *cintillo* revealed that in 14 dpa controls expression extended posteriorly into the pre-existing tissue. As the original pharynx fragment lacked *cintillo* expression, this represents remodeling of pre-existing tissues to an anterior identity. In H,K-ATPase-inhibited regenerates, not only was the expression of *cintillo* greatly reduced (consistent with the shrunken heads), but expression occurred only in new tissues and never below the plane of amputation. Thus, without H,K-ATPase activity the tissue just posterior to the blastema fails to contribute to new head formation. Brain analyses by anti-synapsin labeling revealed similar results. The bi-lobed cephalic ganglia of the planarian brain are marked by the presence of regimented branch domains that extend laterally (Fig. 3D, arrows), distinguishing the brain from the non-branched ganglia of the ventral nerve cords. At 10 dpa, new tissues have lighter staining (presumably from slower peripheral nerve regeneration). In controls at this time point, the new brain was found to extend into original tissues. However, in H,K-ATPase-inhibited regenerates, no cephalic ganglia were observed below the amputation plane. Instead, the brain in shrunken headed regenerates was confined to new tissues, similar to the head marker *cintillo*. Together, these data demonstrate that morphallactic remodeling occurs during head regeneration and that this process requires H,K-ATPase.

Pharynx size and location fail to scale without H,K-ATPase

We next sought to quantify our observations of tiny heads and large, anterior pharynges following H,K-ATPase inhibition, to determine the extent of the remodeling failures. Individual pharynx regenerates were followed from intact worms up to 14 dpa, with both the size and A/P location of the pharynx measured before amputation and after regeneration (Fig. 4A). As expected, overall pharynx size (Fig. 4A, green brackets) decreased in controls, resulting in a smaller pharynx proportional to the smaller worm. In H,K-ATPase-inhibited regenerates, pharynx size failed to reduce, remaining essentially the same size as in the intact worm, producing regenerates with pharynges disproportionately large relative to the smaller body (see also supplementary material Fig. S1B). Similarly, remodeling of the final A/P pharyngeal location (Fig. 4A, yellow brackets) of the regenerate was examined. Whereas pharynx

location in controls was shifted posteriorly towards the center of the A/P axis (concurrent with pharynx resizing), in H,K-ATPase-inhibited regenerates the pharynx failed to shift posteriorly, consistent with the failure in pharynx size reduction. The result was a regenerate with a large pharynx that began just posterior to the head and which extended over much of the body. H,K-ATPase-inhibited regenerates also failed to undergo body elongation, retaining a wide morphology more characteristic of 3-7 dpa regenerates. Together, these data reveal that H,K-ATPase is required for the entire remodeling process: both the early process of pharyngeal size reduction (largely completed by 7 dpa) and the later process of pharyngeal A/P relocation (by 10 dpa), as well as the final process of body elongation (by 17 dpa). This suggests that H,K-ATPase is a very early regulator of the morphallactic process.

Fig. 4.

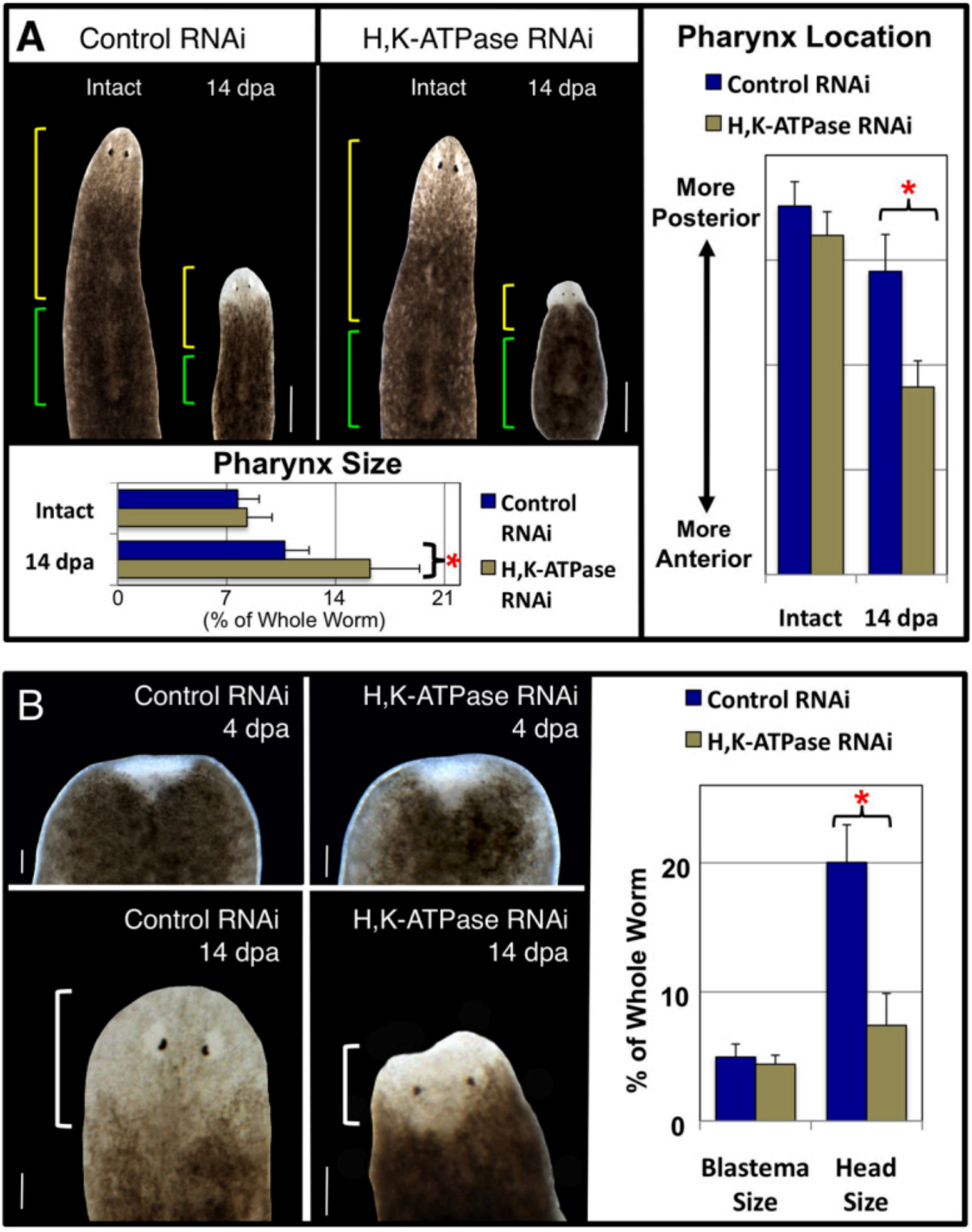

Open in a new tab

H,K-ATPase inhibition prevents tissue remodeling without affecting blastema growth. (**A**) Pharynx remodeling during regeneration. The same planarian shown before amputation and as a 14 dpa pharynx regenerate (composite image). Green brackets, pharynx; yellow brackets, pharynx location on the A/P axis. Average pharynx size: 7.7% (control intact), 8.3% (H,K-ATPase RNAi intact), 10.7% (control 14 dpa), 16.2% (H,K-ATPase RNAi 14 dpa). (**B**) Head remodeling during regeneration. The same tail regenerate (amputated just once posterior to the pharynx) is shown at 4 dpa (top panels) and at 14 dpa (bottom panels). Average blastema size at 4 dpa: 4.9% (control), 4.5% (H,K-ATPase RNAi). Average head size at 14 dpa: 20% (control), 7.5% (H,K-ATPase RNAi). White brackets, head. Anterior is up. $^{*}P<0.0001$. Error bars: s.d. ($n\geq14$). Scale bars: in A, 400 µm; in B, 100 µm.

Without H,K-ATPase, head structures arise from new tissue only

Analyses of the shrunken heads were complicated by the fact that our data revealed that head regeneration comprises both epimorphosis (blastema cells) and morphallaxis (pre-existing cells). To begin separating the contributions of new tissue growth from old tissue remodeling in H,K-ATPase-inhibited regenerates, we examined blastema size prior to the formation of head structures, followed by total head size in the same individuals at the end of regeneration (Fig. 4B). At 4 dpa, blastema size was indistinguishable between controls and *Smed-H¸K-ATPase(RNAi)* regenerates. However, by 14 dpa H,K-ATPase-inhibited regenerates had heads ~50% smaller than controls, consistent with the shrunken head phenotype. Most interestingly, total head size in H,K-ATPase regenerates (at the end of head regeneration) was comparable to the initial size of the blastema (early in regeneration). This suggests that after 4 dpa, head size increases from remodeling of old tissues rather than continued proliferation of blastema cells. These data, together with our previous head domain marker analyses, demonstrate that tissue remodeling of pre-existing tissues just posterior to the blastema is part of head regeneration, as the new blastema growth is not sufficient to replace all missing anterior tissues. Furthermore, in H,K-ATPase-inhibited regenerates all anterior structures are the result of new proliferation, without any contribution from remodeling of existing tissues. These data also suggest that tissue remodeling is not required for the migration and differentiation of eye progenitor cells (Lapan and Reddien, 2011), as *Smed-H¸K-ATPase(RNAi)* regenerates possessed both photoreceptor and pigment cells (supplementary material Fig. S5).

H,K-ATPase does not regulate blastema-associated proliferation

In planarians, new growth arises from proliferation of the neoblasts, which are an adult stem-cell population that comprises ~20% of all cells and the only mitotically active cells in the worm (Gurley and Sánchez Alvarado, 2008; Aboobaker, 2011). Two waves of mitoses occur during regeneration: the first peak (~4 hpa) is an animal-wide injury response associated with neoblast migration to the wound; the second peak (2-3 dpa) occurs at the wound site and is associated with blastema formation and neoblast differentiation (Wenemoser and Reddien, 2010). To determine whether H,K-ATPase inhibition affects new growth, we assessed mitotic activity in *Smed-H¸K-ATPase(RNAi)* regenerates during both mitotic peaks (Fig. 5). Neither the initial animal-wide peak of proliferation (at 4 hpa), nor baseline mitotic activity (restored by 14 dpa), required H,K-ATPase activity. Additionally, the second mitotic peak (at 3 dpa) local to the wound site that promotes blastema outgrowth was also not affected by H,K-ATPase inhibition. This is consistent with our observations that neither blastema formation nor blastema size is altered in *Smed-H¸K-ATPase(RNAi)* regenerates. These data suggest that blastema-associated regenerative growth is not linked to H,K-ATPase activity.

Fig. 5.

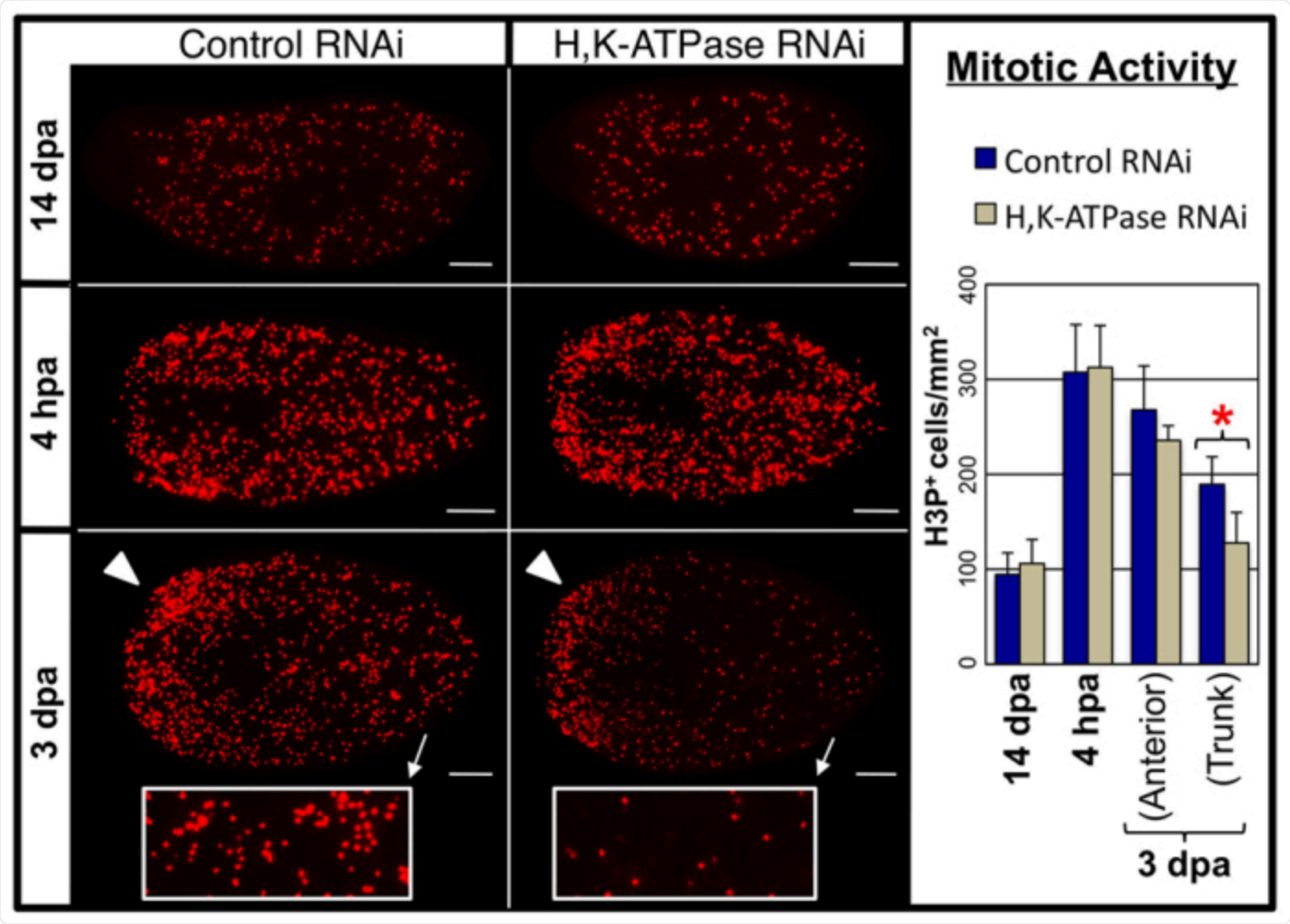

Open in a new tab

H,K-ATPase does not regulate blastema-associated proliferation. Mitotic activity detected by anti-phosphorylated histone H3 (H3P) labeling (headless regenerates, amputated once anterior to pharynx). H,K-ATPase does not affect basal levels of proliferation (re-established by 14 dpa), nor upregulated proliferation in the trunk at 4 hpa, nor at the blastema margin (arrowheads) at 3 dpa. However, H,K-ATPase-inhibited regenerates at 3 dpa have reduced proliferation in the trunk (insets; where remodeling of pre-existing tissues occurs). Anterior is left. $^{*}P<0.01$. Error bars: s.d. ($n\geq7$). Scale bars: 200 µm.

Surprisingly, further analyses of mitotic activity at 3 dpa showed that although anterior proliferation at the wound site was not affected by H,K-ATPase inhibition, proliferation located in the body (trunk) of the

regenerate was reduced (Fig. 5, insets). The upregulated mitoses of the second proliferative peak are normally redistributed more evenly throughout the animal body during subsequent days, perhaps by cell migration (Wenemoser and Reddien, 2010). Our data indicate that this process is H,K-ATPase dependent. Notably, at this point (3 dpa) we observe the start of tissue remodeling in existing tissues, raising the possibility that this redistribution of proliferative cells in the trunk is associated with remodeling events. In conclusion, the data suggest that the H,K-ATPase-independent proliferative injury response and blastema formation occurring early in regeneration are not sufficient to initiate tissue remodeling and scaling, but that later in regeneration initiation of the H,K-ATPase-dependent remodeling process does affect the relocalization of a portion of blastema-driven mitosis into existing tissues.

H,K-ATPase regulates tissue remodeling via control of apoptosis

Our results identify a requirement for H,K-ATPase activity in a majority of morphallactic events during regeneration, including head and pharynx remodeling, body elongation and tissue identity reassignment. We next sought to elucidate the mechanism by which H,K-ATPase ion transport activity regulates organ size and proportion. The scaling of existing tissues to maintain body proportion during regeneration in planarians appears to involve apoptotic tissue remodeling (Pellettieri and Sanchez Alvarado, 2007; Gonzalez-Estevez and Salo, 2010; Pellettieri et al., 2010; Bender et al., 2012), including the caspase family of regulators (Hwang et al., 2004; Gonzalez-Estevez et al., 2007). Apoptosis in planarians undergoes two peaks (inversely localized to the mitotic peaks); the first apoptotic peak (from 1 to 4 hpa) is at the wound site, whereas the second peak (at 3 dpa) is dispersed throughout the animal (Pellettieri et al., 2010).

To ensure that apoptosis is the mechanism driving morphallaxis, we used the apoptosis inhibitor M50054 (Tsuda et al., 2001) to block apoptosis directly without targeting the H,K-ATPase (Fig. 6A). When assessed by activated-caspase-3 activity (an apoptosis marker), we found that M50054 treatment did not inhibit all apoptotic activity, but was sufficient to significantly reduce the amount of apoptosis that occurred (supplementary material Fig. S7). Pharynx fragments treated with M50054 regenerated with smaller heads (Fig. 6A, white brackets) and excessively large pharynges (Fig. 6A, green brackets) that were shifted anteriorly (Fig. 6A, yellow brackets). Thus, knockdown of apoptotic activity results in organ size defect phenotypes that are very similar to H,K-ATPase inhibition, suggesting that H,K-ATPase-dependent tissue remodeling might be mediated by apoptosis.

Fig. 6.

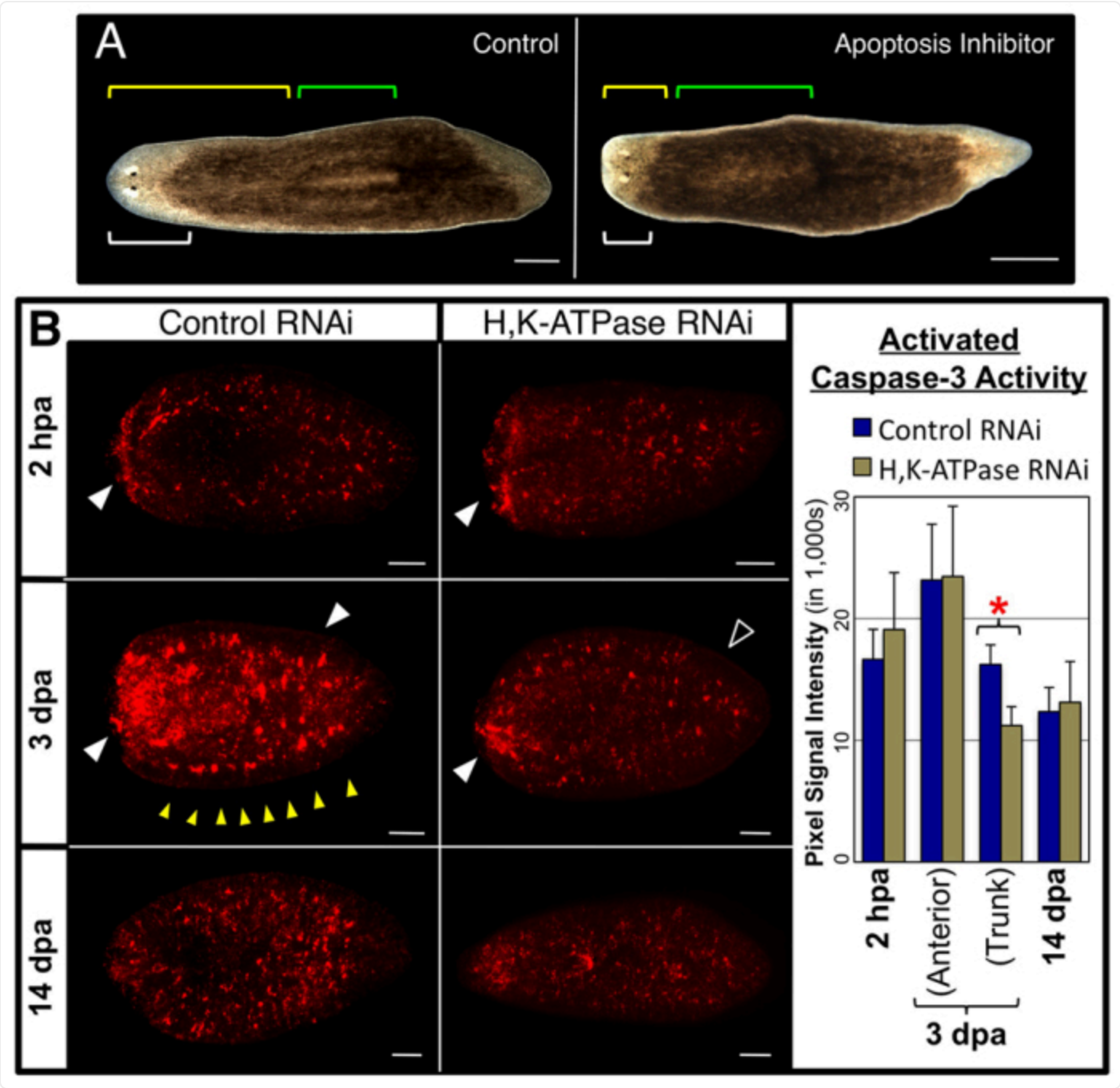

Open in a new tab

H,K-ATPase mediates apoptotic tissue remodeling. (**A**) Pharynx regenerates (14 dpa) treated with the apoptosis inhibitor M50054. White brackets, head; green brackets, pharynx; yellow brackets, pharynx location on the A/P axis. Reduced remodeling: 0% (control), 45% (M50054). $n=40$. (**B**) Apoptosis detected by activated caspase-3 labeling (regenerates amputated once

anterior to the pharynx). H,K-ATPase inhibition does not affect basal levels of apoptosis (restored by 14 dpa), nor upregulated apoptosis at the wound site at 2 hpa. However, at 3 dpa apoptosis in the trunk (associated with remodeling of existing tissues) is blocked in H,K-ATPase-inhibited regenerates (even though upregulated apoptosis near the blastema is unaffected). Filled white arrowheads indicate the presence and unfilled arrowhead the absence of upregulated apoptotic activity. Yellow arrowheads indicate punctate areas of upregulation at the lateral margin. Anterior is left. $^{*}P<0.001$. Error bars: s.d. ($n\geq5$). Scale bars: in B, 200 µm; in A, 400 µm.

To determine whether H,K-ATPase regulates apoptosis in planarians, we assessed activated-caspase-3 activity following *Smed-H¸K-ATPase(RNAi)* injection (Fig. 6B). Loss of H,K-ATPase did not affect basal levels of apoptosis, which are re-established by 14 dpa. Similarly, at 2 hpa, both controls and H,K-ATPase-inhibited regenerates had upregulated activity at the wound site, consistent with the first apoptotic peak. However, at 3 dpa, when the second apoptotic peak occurs, H,K-ATPase-inhibited regenerates failed to upregulate activated-caspase-3 in the trunk. These data demonstrate that H,K-ATPase activity is required to initiate apoptosis during the second peak. The converse experiment, rescue of the H,K-ATPase phenotype by activation of apoptosis (or delivery of recombinant proteins), was hindered by technical limitations (supplementary material Fig. S8). We assiduously attempted gain-of-function techniques (mRNA, recombinant cDNA or bead implantation), but, paralleling the experience of many other groups, found them to be unsuccessful in planarians (supplementary material Fig. S8A). Although pharmacological reagents can activate apoptosis in planarians (supplementary material Fig. S7A), animal-wide exposure for even just 3 hours was 100% lethal ($n=40$). These data are consistent with the lethality reported following *Smed-BCL2(RNAi)* injection, which similarly activates global apoptosis (Pellettieri et al., 2010). Localized activation of apoptosis by heated needle stabbings, as described for hydra (Chera et al., 2009), was less lethal (30%), but this caused upregulated apoptosis for <24 hours and failed to rescue the H,K-ATPase phenotype (supplementary material Fig. S8B). Longer periods of carefully patterned, tissue-specific apoptosis are likely to be required to remodel planarian organs.

Our data suggest that the second peak of apoptosis at 3 dpa functions to drive the remodeling of existing tissues (as 3 dpa is when morphallaxis is first observed) and demonstrate that H,K-ATPase is required for this remodeling-associated apoptosis to occur. Interestingly, as with proliferation, *Smed-H¸K-ATPase(RNAi)* injection had no effect on the upregulation of activated-caspase-3 activity near the wound at 3 dpa (Fig. 6B), perhaps suggesting that continued apoptosis at the site of blastema outgrowth is unconnected to remodeling events. Together, the data show that H,K-ATPase mediates tissue remodeling during regeneration through regulation of apoptosis.

DISCUSSION

Our data reveal that the H,K-ATPase ion pump is required for apoptosis-mediated head size and organ scaling throughout the animal. Morphallactic defects in *Smed-H,K-ATPase(RNAi)* regenerates were observed in: head and pharyngeal resizing; pharyngeal A/P placement; anterior neural, brain and intestinal tract remodeling; and the re-establishment of anterior identity in previously more posterior tissues. All these remodeling defects occurred without inhibiting new tissue proliferation associated with blastema growth (epimorphosis). Therefore, when H,K-ATPase is lost during regeneration, head is made from new tissues and stays small because remodeling failures prevent old tissues from contributing to it, whereas the pharynx stays large because apoptosis fails to sculpt it to the correct size. This suggests that morphallactic remodeling of pre-existing tissues is an independent pathway from epimorphic blastema growth, a distinction that was previously unclear (Agata et al., 2007).

The working definitions used here for epimorphosis (proliferation-driven blastema formation) and morphallaxis (apoptotic-driven cell rearrangements of the original fragment accomplished mainly without new proliferation) were of necessity rather simple. Apoptosis appears to be central to both processes, as does cell migration. The data do not rule out the possibility that either 'new' cells from the blastema migrate into existing tissues or conversely that 'old' cells from the trunk enter the blastema, and evidence suggests that such cell migration might occur. Amputation triggers neoblast migration to the site of injury (Guedelhoefer and Alvarado, 2012), whereas proliferation at the wound site results in stem-cell prodigy that disperse throughout the blastema (Eisenhoffer et al., 2008). At 3 dpa, the second peak of mitosis at the wound site gets 're-distributed' throughout the trunk during subsequent days, perhaps through stem cell migration (Pellettieri et al., 2010). Our data shows that this redistribution fails to occur when H,K-ATPase-dependent remodeling is inhibited (Fig. 5). Although our data demonstrate that blastema formation does not automatically lead to tissue remodeling, this does not exclude a requirement for growth in initiating remodeling, although studies to date present conflicting evidence. Although neoblast proliferation is required for intestinal remodeling in planarians (Forsthoefel et al., 2011), both the first and second apoptotic peaks are stem cell independent and occur in neoblast-ablated regenerates (Pellettieri et al., 2010). Together, our data indicate that planarian regeneration is the result of careful coordination between both new proliferation and tissue remodeling, as seen in the intestinal tract, where regeneration in existing tissues comprises both H,K-ATPase-independent proliferation (of anterior and some secondary branches) and H,K-ATPase-dependent remodeling of pre-existing tissues (to form tertiary and quaternary branches).

All the data suggest that 3 dpa is a benchmark for tissue remodeling during planarian regeneration. In our analyses, no remodeling was observed prior to 3 dpa. Interestingly, for chemical inhibition of H,K-ATPase (with SCH-28080) to block remodeling, planarians must be exposed until the end of 3 dpa

(Beane et al., 2011). The data lead to the following sequential model (Fig. 7): at 1-4 hpa, injury-induced apoptosis occurs at the wound site (Pellettieri et al., 2010), followed by an animal-wide proliferative peak from 4 to 6 hpa (Wenemoser and Reddien, 2010). By 24 hpa, upregulated H,K-ATPase expression in the anterior blastema leads to strong membrane depolarization, which must be maintained at least through the end of 3 dpa for remodeling to occur. At 3 dpa, apoptosis is upregulated at the blastema border, which may indicate that apoptosis-induced compensatory proliferation drives the concurrent second proliferative peak in the same region (Wenemoser and Reddien, 2010). [From 3 to 10 dpa, this peak of proliferation at the wound site becomes redistributed throughout existing tissues (Wenemoser and Reddien, 2010).] The second apoptotic peak occurs throughout the animal at 3 dpa (Pellettieri et al., 2010), coinciding with when tissue remodeling was first observed in regenerates. From 3 to 7 dpa, the pharynx is resized and a first wave of body elongation occurs, whereas from 3 to 10 dpa the pharynx is relocated on the A/P axis. Head resizing occurs from 10 dpa onwards. A second wave of body elongation occurs at 14-17 dpa, resulting a new smaller worm proportionally similar to the original worm prior to amputation. Together, the data strongly suggest that the crucial time during which tissue remodeling and scaling is initiated is on day 3 of regeneration.

Fig. 7.

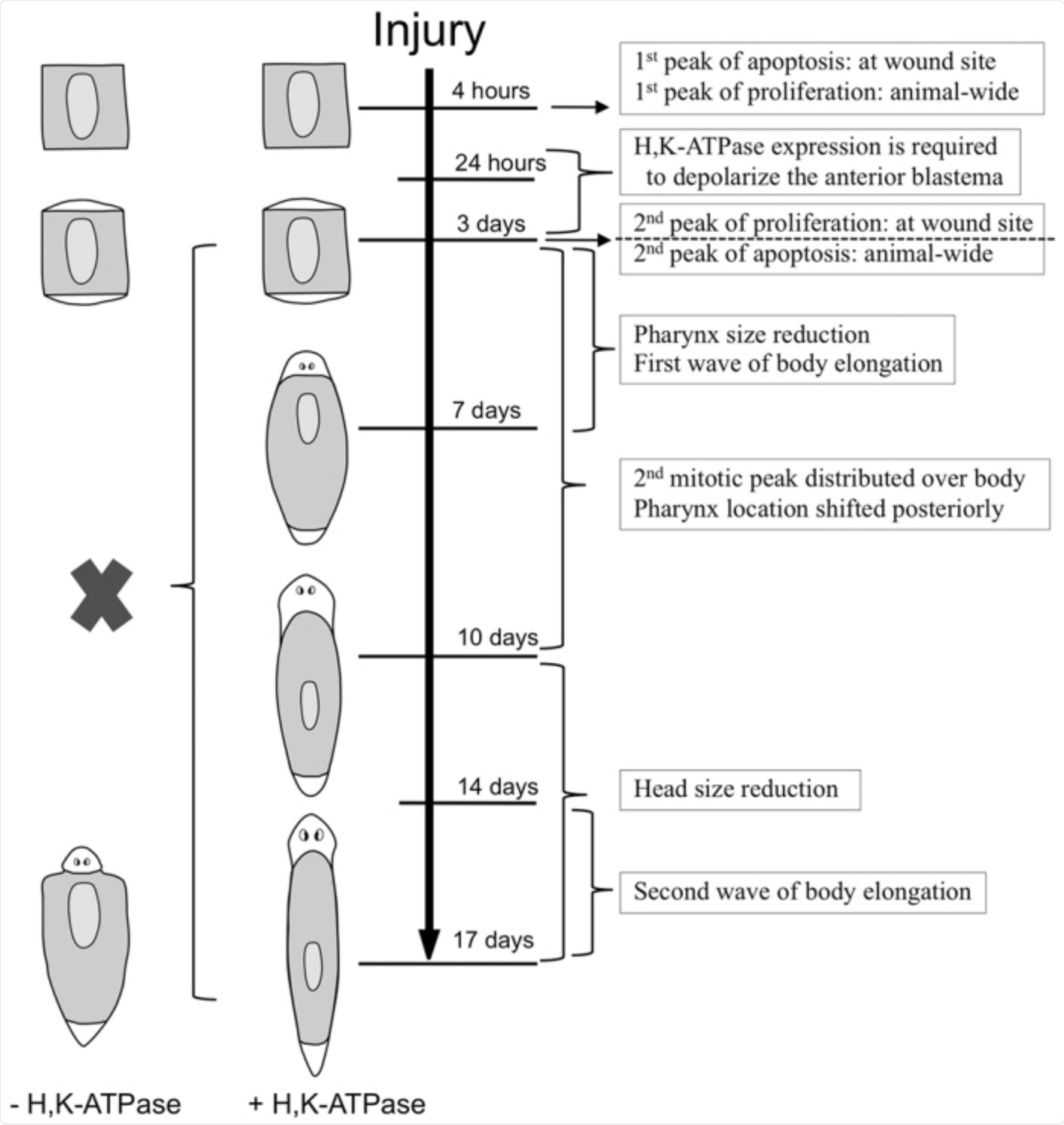

Open in a new tab

Model of H,K-ATPase-mediated tissue remodeling during regeneration. Timeline of events. White tissues, new growth (blastema); shaded tissues, pre-existing tissues. All events below the

dashed line are dependent on H,K-ATPase activity (blockade of which is indicated by the black cross).

None of the events prior to 3 dpa is H,K-ATPase-dependent, whereas all of the events from 3 dpa to the end of regenerative tissue remodeling require H,K-ATPase activity. We have shown that H,K-ATPase-mediated anterior membrane depolarization is required for correct anatomical polarity of the blastema (Beane et al., 2011), providing a bioelectrical link between determination of regional identity and morphological sculpting. This might indicate that H,K-ATPase-regulated membrane voltage is required only through 3 dpa to initiate tissue remodeling. However, we observed punctate regions of activated-caspase-3 in the lateral margins at 3 dpa (Fig. 6B, yellow arrowheads), reminiscent of the punctuate H,K-ATPase expression pattern in the same region (where H,K-ATPase activity does not lead to strong depolarization). Caspase-3 activation (mediated by H,K-ATPase) in this region could have non-apoptotic remodeling functions, such as during neural synaptic plasticity (Snigdha et al., 2012), perhaps suggesting an additional requirement for H,K-ATPase activity later in regeneration.

Bioelectric cues, because they can function across entire organs, are ideal mechanisms for the orchestration of cell-level activities (e.g. proliferation and apoptosis) into animal-wide organization such as allometric tissue scaling (Levin, 2012). Previous work has proposed voltage gradients as mechanisms for sensing and regulating size (Moment, 1949), establishing positional information (Shi and Borgens, 1995), and pre-patterning naïve cell fields (Burr and Northrop, 1935; Vandenberg et al., 2011). This is the first molecular identification of a specific ion translocator necessary for shape control during regeneration and the mechanism by which it sculpts the necessary geometrical changes underlying dynamic remodeling. Further studies are needed to delineate whether H,K-ATPase ion transport functions are required at multiple times during remodeling, or whether the H,K-ATPase is required only early in a sequential remodeling process that will occur without further input. The latter hypothesis suggests that bioelectric control of apoptosis might function as a kind of master switch, and need only be turned on for the remodeling process to initiate and complete. Whether by such master-regulator initiation, or by facilitating specific regional control over apoptotic remodeling, genetic and pharmacological regulation of native ion flux is an exciting new approach for pattern regulation. Understanding and learning to manipulate the biophysical processes that guide living growth and form will have broad and significant implications for bioengineering, synthetic biology and the translation of regenerative therapies.

Supplementary Material

Supplementary Material

supp_140_2_313__index.html (720B, html)

Acknowledgments

We thank A.-S. Tseng for manuscript suggestions; T. Shomrat and D. Blackiston for assistance with behavioral assays; D. Adams for assistance with reporter dyes; C. Stevenson for cloning assistance; and B. Chernet for GFP reagents. W.S.B. thanks J. Beane and S. Beane for continued support.

Footnotes

Funding

M.L. gratefully acknowledges support by the Mathers Foundation; a National Science Foundation (NSF) grant [IBN# 0347295]; a National Highway Traffic Safety Administration (NHTSA) grant [DTNH22-06-G-00001]; and a National Institutes of Health (NIH) grant [HD055850]. Deposited in PMC for release after 12 months.

Competing interests statement

The authors declare no competing financial interests.

Supplementary material

Supplementary material available online at
http://dev.biologists.org/lookup/suppl/doi:10.1242/dev.086900/-/DC1

References

1. Aboobaker A. A. (2011). Planarian stem cells: a simple paradigm for regeneration. *Trends Cell Biol.* 21, 304–311 [DOI] [PubMed] [Google Scholar]

2. Agata K., Saito Y., Nakajima E. (2007). Unifying principles of regeneration I: Epimorphosis versus morphallaxis. *Dev. Growth Differ.* 49, 73–78 [DOI] [PubMed] [Google Scholar]

3. Beane W. S., Morokuma J., Adams D. S., Levin M. (2011). A chemical genetics approach reveals H,K-ATPase-mediated membrane voltage is required for planarian head regeneration. *Chem. Biol.* 18, 77–89 [DOI] [PMC free article] [PubMed] [Google Scholar]

4. Beane W. S., Tseng A. S., Morokuma J., Lemire J. M., Levin M. (2012). Inhibition of planar cell polarity extends neural growth during regeneration, homeostasis, and development. *Stem Cells Dev.* 21, 2085–2094 [DOI] [PMC free article] [PubMed] [Google Scholar]

5. Bender C. E., Fitzgerald P., Tait S. W., Llambi F., McStay G. P., Tupper D. O., Pellettieri J., Sanchez Alvarado A., Salvesen G. S., Green D. R. (2012). Mitochondrial pathway of apoptosis is ancestral in metazoans. *Proc. Natl. Acad. Sci. USA* 109, 4904–4909 [DOI] [PMC free article] [PubMed] [Google Scholar]

6. Blackiston D., Shomrat T., Nicolas C. L., Granata C., Levin M. (2010). A second-generation device for automated training and quantitative behavior analyses of molecularly-tractable model organisms. *PLoS ONE* 5, e14370 [DOI] [PMC free article] [PubMed] [Google Scholar]

7. Burr H. S., Northrop F. S. C. (1935). The electro-dynamic theory of life. *Q. Rev. Biol.* 10, 322–333 [Google Scholar]

8. Cebria F., Newmark P. A. (2005). Planarian homologs of netrin and netrin receptor are required for proper regeneration of the central nervous system and the maintenance of nervous system architecture. *Development* 132, 3691–3703 [DOI] [PubMed] [Google Scholar]

9. Chera S., Ghila L., Dobretz K., Wenger Y., Bauer C., Buzgariu W., Martinou J. C., Galliot B. (2009). Apoptotic cells provide an unexpected source of Wnt3 signaling to drive hydra head regeneration. *Dev. Cell* 17, 279–289 [DOI] [PubMed] [Google Scholar]

10. Corpet F. (1988). Multiple sequence alignment with hierarchical clustering. *Nucleic Acids Res.* 16, 10881–10890 [DOI] [PMC free article] [PubMed] [Google Scholar]

11. Egeblad M., Rasch M. G., Weaver V. M. (2010). Dynamic interplay between the collagen scaffold and tumor evolution. *Curr. Opin. Cell Biol.* 22, 697–706 [DOI] [PMC free article] [PubMed] [Google Scholar]

12. Eisenhoffer G. T., Kang H., Sanchez Alvarado A. (2008). Molecular analysis of stem cells and their descendants during cell turnover and regeneration in the planarian Schmidtea

mediterranea. *Cell Stem Cell* 3, 327–339 [DOI] [PMC free article] [PubMed] [Google Scholar]

13. Forsthoefel D. J., Park A. E., Newmark P. A. (2011). Stem cell-based growth, regeneration, and remodeling of the planarian intestine. *Dev. Biol.* 356, 445–459 [DOI] [PMC free article] [PubMed] [Google Scholar]

14. Fuchs Y., Steller H. (2011). Programmed cell death in animal development and disease. *Cell* 147, 742–758 [DOI] [PMC free article] [PubMed] [Google Scholar]

15. Gonzalez-Estevez C., Salo E. (2010). Autophagy and apoptosis in planarians. *Apoptosis* 15, 279–292 [DOI] [PubMed] [Google Scholar]

16. Gonzalez-Estevez C., Felix D. A., Aboobaker A. A., Salo E. (2007). Gtdap-1 promotes autophagy and is required for planarian remodeling during regeneration and starvation. *Proc. Natl. Acad. Sci. USA* 104, 13373–13378 [DOI] [PMC free article] [PubMed] [Google Scholar]

17. Gosman J. H., Stout S. D., Larsen C. S. (2011). Skeletal biology over the life span: a view from the surfaces. *Am. J. Phys. Anthropol.* 146 Suppl. 53, 86–98 [DOI] [PubMed] [Google Scholar]

18. Guedelhoefer O. C., IV, Alvarado A. S. (2012). Amputation induces stem cell mobilization to sites of injury during planarian regeneration. *Development* 139, 3510–3520 [DOI] [PMC free article] [PubMed] [Google Scholar]

19. Gurley K. A., Sánchez Alvarado A. (2008). Stem cells in animal models of regeneration, doi/10.3824/stembook.1.32.1, http://www.stembook.org [PubMed]

20. Hicks C., Sorocco D., Levin M. (2006). Automated analysis of behavior: a computer-controlled system for drug screening and the investigation of learning. *J. Neurobiol.* 66, 977–990 [DOI] [PubMed] [Google Scholar]

21. Huang Y. L., Chuang C. Y., Sung F. C., Chen C. Y. (2008). Thioredoxin overexpression modulates remodeling factors in stress responses to cigarette smoke. *J. Toxicol. Environ. Health A* 71, 1490–1498 [DOI] [PubMed] [Google Scholar]

22. Hwang J. S., Kobayashi C., Agata K., Ikeo K., Gojobori T. (2004). Detection of apoptosis during planarian regeneration by the expression of apoptosis-related genes and TUNEL assay. *Gene* 333, 15–25 [DOI] [PubMed] [Google Scholar]

23. Lapan S. W., Reddien P. W. (2011). dlx and sp6-9 Control optic cup regeneration in a prototypic eye. *PLoS Genet.* 7, e1002226 [DOI] [PMC free article] [PubMed] [Google Scholar]

24. Levin M. (2012). Molecular bioelectricity in developmental biology: New tools and recent discoveries: Control of cell behavior and pattern formation by transmembrane potential gradients. *BioEssays* 34, 205–217 [DOI] [PMC free article] [PubMed] [Google Scholar]

25. Moment G. B. (1949). On the relation between growth in length, the formation of new segments, and electric potential in an earthworm. *J. Exp. Zool.* 112, 1–12 [DOI] [PubMed] [Google Scholar]

26. Morgan T. H. (1901). *Regeneration*. New York: MacMillan; [Google Scholar]

27. Newmark P. A., Alvarado A. S. (2001). Regeneration in Planaria. In *eLS*. Chichester: John Wiley; [Google Scholar]

28. Nishimura K., Kitamura Y., Inoue T., Umesono Y., Sano S., Yoshimoto K., Inden M., Takata K., Taniguchi T., Shimohama S., et al. (2007). Reconstruction of dopaminergic neural network and locomotion function in planarian regenerates. *Dev. Neurobiol.* 67, 1059–1078 [DOI] [PubMed] [Google Scholar]

29. Nowotschin S., Hadjantonakis A. K. (2010). Cellular dynamics in the early mouse embryo: from axis formation to gastrulation. *Curr. Opin. Genet. Dev.* 20, 420–427 [DOI] [PMC free article] [PubMed] [Google Scholar]

30. Oviedo N. J., Levin M. (2007). smedinx-11 is a planarian stem cell gap junction gene required for regeneration and homeostasis. *Development* 134, 3121–3131 [DOI] [PubMed] [Google Scholar]

31. Oviedo N. J., Newmark P. A., Sanchez Alvarado A. (2003). Allometric scaling and proportion regulation in the freshwater planarian Schmidtea mediterranea. *Dev. Dyn.* 226, 326–333 [DOI] [PubMed] [Google Scholar]

32. Oviedo N. J., Nicolas C. L., Adams D. S., Levin M. (2008). Gene knockdown in planarians using RNA interference. *CSH Protoc.* 2008, doi: 10.1101/pdb prot5054 [DOI] [PMC free article] [PubMed] [Google Scholar]

33. Pastor-Pareja J. C., Grawe F., Martin-Blanco E., Garcia-Bellido A. (2004). Invasive cell behavior during Drosophila imaginal disc eversion is mediated by the JNK signaling cascade.

Dev. Cell 7, 387–399 [DOI] [PubMed] [Google Scholar]

34. Pearson B. J., Eisenhoffer G. T., Gurley K. A., Rink J. C., Miller D. E., Sanchez Alvarado A. (2009). Formaldehyde-based whole-mount in situ hybridization method for planarians. *Dev. Dyn.* 238, 443–450 [DOI] [PMC free article] [PubMed] [Google Scholar]

35. Pellettieri J., Sanchez Alvarado A. (2007). Cell turnover and adult tissue homeostasis: from humans to planarians. *Annu. Rev. Genet.* 41, 83–105 [DOI] [PubMed] [Google Scholar]

36. Pellettieri J., Fitzgerald P., Watanabe S., Mancuso J., Green D. R., Sanchez Alvarado A. (2010). Cell death and tissue remodeling in planarian regeneration. *Dev. Biol.* 338, 76–85 [DOI] [PMC free article] [PubMed] [Google Scholar]

37. Petersen C. P., Reddien P. W. (2008). Smed-betacatenin-1 is required for anteroposterior blastema polarity in planarian regeneration. *Science* 319, 327–330 [DOI] [PubMed] [Google Scholar]

38. Petersen C. P., Reddien P. W. (2009). A wound-induced Wnt expression program controls planarian regeneration polarity. *Proc. Natl. Acad. Sci. USA* 106, 17061–17066 [DOI] [PMC free article] [PubMed] [Google Scholar]

39. Reddien P. W. (2011). Constitutive gene expression and the specification of tissue identity in adult planarian biology. *Trends Genet.* 27, 277–285 [DOI] [PMC free article] [PubMed] [Google Scholar]

40. Robb S. M., Ross E., Sanchez Alvarado A. (2008). SmedGD: the Schmidtea mediterranea genome database. *Nucleic Acids Res.* 36, D599–D606 [DOI] [PMC free article] [PubMed] [Google Scholar]

41. Rydell-Tormanen K., Risse P. A., Kanabar V., Bagchi R., Czubryt M. P., Johnson J. R. (2012). Smooth muscle in tissue remodeling and hyper-reactivity: Airways and arteries. *Pulm. Pharmacol. Ther.* 2012, doi: 10.1016/j.pupt.2012.04.00 [DOI] [PubMed] [Google Scholar]

42. Shi R., Borgens R. B. (1995). Three-dimensional gradients of voltage during development of the nervous system as invisible coordinates for the establishment of embryonic pattern. *Dev. Dyn.* 202, 101–114 [DOI] [PubMed] [Google Scholar]

43. Snigdha S., Smith E. D., Prieto G. A., Cotman C. W. (2012). Caspase-3 activation as a bifurcation point between plasticity and cell death. *Neurosci. Bull.* 28, 14–24 [DOI] [PMC free article] [PubMed] [Google Scholar]

44. Stevenson C. G., Beane W. S. (2010). A low percent ethanol method for immobilizing planarians. *PLoS ONE* 5, e15310 [DOI] [PMC free article] [PubMed] [Google Scholar]

45. Tseng A. S., Adams D. S., Qiu D., Koustubhan P., Levin M. (2007). Apoptosis is required during early stages of tail regeneration in Xenopus laevis. *Dev. Biol.* 301, 62–69 [DOI] [PMC free article] [PubMed] [Google Scholar]

46. Tsuda T., Ohmori Y., Muramatsu H., Hosaka Y., Takiguchi K., Saitoh F., Kato K., Nakayama K., Nakamura N., Nagata S., et al. (2001). Inhibitory effect of M50054, a novel inhibitor of apoptosis, on anti-Fas-antibody-induced hepatitis and chemotherapy-induced alopecia. *Eur. J. Pharmacol.* 433, 37–45 [DOI] [PubMed] [Google Scholar]

47. Vandenberg L. N., Morrie R. D., Adams D. S. (2011). V-ATPase-dependent ectodermal voltage and pH regionalization are required for craniofacial morphogenesis. *Dev. Dyn.* 240, 1889–1904 [DOI] [PMC free article] [PubMed] [Google Scholar]

48. Wagner D. E., Wang I. E., Reddien P. W. (2011). Clonogenic neoblasts are pluripotent adult stem cells that underlie planarian regeneration. *Science* 332, 811–816 [DOI] [PMC free article] [PubMed] [Google Scholar]

49. Wagner D. E., Ho J. J., Reddien P. W. (2012). Genetic regulators of a pluripotent adult stem cell system in planarians identified by RNAi and clonal analysis. *Cell Stem Cell* 10, 299–311 [DOI] [PMC free article] [PubMed] [Google Scholar]

50. Wenemoser D., Reddien P. W. (2010). Planarian regeneration involves distinct stem cell responses to wounds and tissue absence. *Dev. Biol.* 344, 979–991 [DOI] [PMC free article] [PubMed] [Google Scholar]

51. Wenemoser D., Lapan S. W., Wilkinson A. W., Bell G. W., Reddien P. W. (2012). A molecular wound response program associated with regeneration initiation in planarians. *Genes Dev.* 26, 988–1002 [DOI] [PMC free article] [PubMed] [Google Scholar]

Associated Data

This section collects any data citations, data availability statements, or supplementary materials included in this article.

Supplementary Materials

Supplementary Material

supp_140_2_313__index.html (720B, html)

supp_140.2.313_DEV086900.pdf (1.7MB, pdf)